Title

DiSCoVERing Innovative Therapies for Rare Tumors: Combining Genetically Accurate Disease Models with In Silico Analysis to Identify Novel Therapeutic Targets

Journal

Clinical Cancer Research, 22(15)

ISSN

1078-0432

Authors

Hanaford, Allison R
Archer, Tenley C
Price, Antoinette
et al.

Publication Date

2016-08-01

DOI

10.1158/1078-0432.ccr-15-3011

Peer reviewed

HHS Public Access

Author manuscript

Clin Cancer Res. Author manuscript; available in PMC 2017 August 01.

Published in final edited form as:

Clin Cancer Res. 2016 August 1; 22(15): 3903–3914. doi:10.1158/1078-0432.CCR-15-3011.

DiSCoVERing innovative therapies for rare tumors: combining genetically accurate disease models with *in silico* analysis to identify novel therapeutic targets

Allison Hanaford[1], **Tenley C Archer**[2,3], **Antoinette Price**[1], **Ulf D. Kahlert**[4], **Jarek Maciaczyk**[4], **Guido Nikkhah**[5], **Jong Wook Kim**[2,6], **Tobias Ehrenberger**[2,7], **Paul A. Clemons**[2,8], **Vlado Dančík**[8], **Brinton Seashore-Ludlow**[8], **Vasanthi Viswanathan**[8], **Michelle L Stewart**[8], **Matthew G. Rees**[8], **Alykhan Shamji**[8], **Stuart Schreiber**[2,8,9,10], **Ernest Fraenkel**[2,7], **Scott L Pomeroy**[2,3], **Jill P Mesirov**[2,11,12], **Pablo Tamayo**[2,11,12], **Charles Eberhart**[1], and **Eric Raabe**[1,13]

[1]Department of Pathology, Johns Hopkins School of Medicine, Baltimore MD

[2]Eli and Edythe Broad Institute of MIT and Harvard, Cambridge, MA

[3]Department of Neurology, Boston Children's Hospital, Harvard Medical School, Cambridge, MA

[4]Department of Neurosurgery, Heinrich-Heine University Hospital Duesseldorf, Germany

[5]Department of Neurosurgery, University Hospital Stuttgart, Germany

[6]Department of Medical Oncology, Dana-Farber Cancer Institute, Boston MA

[7]Department of Biological Engineering, Massachusetts Institute of Technology, Cambridge, MA

[8]Center for the Science of Therapeutics, Broad Institute, Cambridge, MA

[9]Department of Chemistry and Chemical Biology, Harvard University, Cambridge, MA

[10]Howard Hughes Medical Institute

[11]Department of Medicine, UC San Diego, La Jolla, CA

[12]Moores Cancer Center, UC San Diego, La Jolla, CA

[13]Division of Pediatric Oncology, Johns Hopkins School of Medicine, Baltimore MD

Abstract

Purpose—We used human stem and progenitor cells to develop a genetically accurate novel model of MYC-driven Group 3 medulloblastoma. We also developed a new informatics method, Disease-model Signature vs. Compound-Variety Enriched Response ("DiSCoVER"), to identify novel therapeutics that target this specific disease subtype.

Experimental Design—Human neural stem and progenitor cells derived from the cerebellar anlage were transduced with oncogenic elements associated with aggressive medulloblastoma. An

Corresponding authors: Eric Raabe, Division of Pediatric Oncology, Bloomberg 11379, 1800 Orleans, Johns Hopkins Hospital, Baltimore, MD 21287, eraabe2@jhmi.edu and Charles G. Eberhart, Department of Pathology, Johns Hopkins University School of Medicine, 720 Rutland Ave, Ross Bldg, 558, Baltimore, MD 21205. ceberha@jhmi.edu.

The authors report no conflict of interest

in silico analysis method for screening drug sensitivity databases (DiSCoVER) was used in multiple drug sensitivity datasets. We validated the top hits from this analysis *in vitro* and *in vivo*.

Results—Human neural stem and progenitor cells transformed with c-MYC, dominant-negative p53, constitutively active AKT and hTERT formed tumors in mice that recapitulated Group 3 medulloblastoma in terms of pathology and expression profile. DiSCoVER analysis predicted that the aggressive MYC-driven Group 3 medulloblastoma would be sensitive to CDK inhibitors. The CKD4/6 inhibitor palbociclib decreased proliferation, increased apoptosis and significantly extended the survival of mice with orthotopic medulloblastoma orthotopic xenografts.

Conclusion—We present a new method to generate genetically accurate models of rare tumors, and a companion computational methodology to find therapeutic interventions that target them. We validated our human neural stem cell model of MYC-driven Group 3 medulloblastoma and showed that CDK4/6 inhibitors are active against this subgroup. Our results suggest that palbociclib is a potential effective treatment for poor-prognosis MYC-driven Group 3 medulloblastoma tumors in carefully selected patients.

Introduction

Our knowledge of the biology of rare tumors and the development of new therapies is hampered by the lack of biologically relevant or genetically and functionally accurate models. Patient-derived tumor cell lines may be difficult, if not impossible, to grow in culture (1), and even if cell lines can be maintained in culture, high serum or other *in vitro* conditions can result in genetic changes that diverge from the original tumor, reducing the cell line's utility as a model (2). Serial xenografts from primary human tumors represent another promising approach (3), but because cultured cells and serial xenografts are often genetically complex, it can be difficult to elucidate the key drivers of tumor formation.

Mouse models have led to great advances in our understanding of the biology of a variety of tumors. However, murine cells are not always transformed in a fashion equivalent to human ones (4), and expression profiles can be challenging to reconcile between mouse and human. We propose an alternative strategy starting with a human tissue of origin and adding or ablating hypothesized key genetic drivers of the tumor of interest to allow the creation of a more genetically and functionally accurate system to study the biology of cancer (Figure 1A). These transformed isogenic model systems could also be useful tools to test the efficacy of novel therapeutics.

To investigate this strategy, we used cerebellar-derived human neural stem cells to model the cerebellar neoplasm medulloblastoma, which is the most common of malignant pediatric brain tumor. Standard treatment consists of surgical resection, radiation and chemotherapy and results in a 60 to 70% long term survival. Traditional criteria for poor prognosis included large cell/anaplastic histology, metastatic disease, or significant post-operative residual tumor (5). MYC expression positively correlates with anaplasia and poor outcome (6–8). RNA expression profiling, copy number analysis, genome sequencing, and DNA methylation studies have subdivided medulloblastoma into molecular subgroups (9–12). The current consensus consists of four molecular subgroups: WNT, SHH, Group 3 and Group 4 (11), however, a previous study analyzing larger cohorts proposed six molecular subgroups

—C1 through C6 (referred to here as the Cho *et al.* subgroups) (12). The Cho *et al.* subgroups are almost perfectly nested in the four consensus groups in such way that groups C1 and C5 comprise consensus Group 3.

A key feature of Group 3/C1 medulloblastoma is high expression of MYC. The C1 subgroup therefore consists of MYC-amplified or MYC up-regulated poor prognosis tumors (12). These aggressive malignancies frequently metastasize to the leptomeningeal space and spine and have the worst outcome (5, 10, 12, 13). Improved therapeutic strategies are urgently needed for this subgroup. In many cases, increased levels of *MYC* mRNA are associated with DNA amplicons at this locus (7), but in other tumors the precise cause of MYC upregulation remains unknown. Increased MYC expression can promote medulloblastoma formation and results in an anaplastic tumor phenotype (6, 14, 15). Suppressing MYC or its cofactors can slow medulloblastoma growth (16). Regardless of subgroup, the hallmarks of recurrent medulloblastoma include mutation in *TP53* and increased MYC expression (17).

A number of patient derived medulloblastoma cell lines exist, some of which have *MYC* amplicons (18). Two groups have used mouse cerebellar stem or progenitor cells to study the role of MYC in promoting the initiation and growth of Group 3 medulloblastoma (14, 15). These *MYC* overexpression and *TP53* abrogated xenografts form aggressive tumors that histologically and molecularly resembled human group 3 medulloblastoma (14, 15). Increased MYCN expression can also promote medulloblastoma formation (19). MYCN-driven murine transgenic medulloblastoma may represent a better molecular match for human Group 3 tumors than MYC-driven approaches, despite the fact that MYCN is most prominent in other medulloblastoma subgroups (20), illustrating the problems that arise when using mouse cells to study a human disease.

The poor prognosis and high morbidity of Group 3/C1 medulloblastoma drive the search for new therapeutic strategies for this aggressive disease subtype. A human neural stem cell model of medulloblastoma that faithfully recapitulates the overall oncogenic state of these tumors can be a powerful tool. An additional motivation for this strategy is the fact that medulloblastoma tumors are genetically relatively simple, having 5 to 10-fold fewer mutations than adult solid tumors (21), making them an ideal choice for our approach.

Methods

Generation of CB NSC Model

Human cerebellar neural stem cells were derived as described (22) and obtained in concordance with German law and Ethics Board evaluation. The study was also approved by the Johns Hopkins Institutional Review Board. The cells were obtained by dissecting the cerebellar anlage and were cultured as neurospheres. Cells were transduced using lentiviral and retroviral vectors. The R248W-TP53 plasmid (Addgene plasmid 16437) and MYC plasmid (Addgene plasmid 17758) were subcloned into pWPI (Addgene 12254) (23). For hTERT and constitutively active AKT, Addgene plasmids 12245 and 15294 were used. The SV40 plasmid is described in Raabe *et al* (24). Lentivirus was produced by transfecting 293T cells with VSV-G envelope plasmid, Δ8.9 gag/pol plasmid and the plasmid containing the gene of interest as described in (24) using FuGENE (Roche) per manufacturer's

instruction. Retrovirus was produced by transfecting 293T-GP cells with VSV-G plasmid and the plasmid containing the gene of interest using FuGENE. 24 hours post transfection, 293T cells were switched to EGF-FGF media and the supernatant was collected at 48 and 72h. The collected supernatant was filtered with a 0.45 micron filter and stored at −80C until use.

Cerebellar neural stem cells were dissociated using Accutase (Sigma) and gentle tituration, then incubated with viral MYC; SV40; or MYC, hTERT and DNp53 viral supernatants for 24 hours. After approximately one week in culture, spheres were identified and individually placed into wells of a 24-well plates. Expression of the introduced oncogenes was verified by western blot and qPCR. Cells successfully transduced with MYC, hTERT and DN-p53 were then incubated with AKT viral supernatant for 24 hours. The cells were then placed under puromycin selection for 72 hours, following which sub-clones were generated as described above.

Cell culture

The human medulloblastoma cell lines D425Med and D238Med were both established at Duke University (18). D283Med is available through ATCC. Both lines are cultured in MEM media supplemented with 10% FBS. The neural stem cell lines grow as neurospheres in media composed of 30% Ham's F12, 70% DMEM, 1% antibiotic antimycotic, 20% B27 supplement, 5ug/mL heparin, 20ng/mL EGF, and 20ng/mL FGF2. Lines transformed with AKT are grown under puromycin selection. All cells were verified to be mycoplasma free by PCR testing. Cell lines were authenticated by STR DNA identity testing by the Johns Hopkins Genetic Resources Core Facility

Histology

Brains were removed from mice immediately following euthanasia and fixed in 10% buffered formalin. The brains were processed and H&E slides prepared by the Johns Hopkins Pathology Reference Lab.

Immunohistochemistry/TMA

IHC was performed on deparaffinized sections of brain xenografts as described (23). The following primary antibodies were used: human specific NESTIN (1:500; Millipore, #MAB5326); GFAP (1:1000; DAKO #Z0334); MAP2 (Santa Cruz #20172); MYC (1:300, Epitomics #14721); phospho-AKT (1:50, Cell Signaling Technologies); TP53 (Sigma, #BP-5312), phospho-RB (1:250, Cell Signaling Technologies #D20B12). For the TMA of 65 primary medulloblastoma samples, IHC was performed on deparaffinized arrays followed by antigen retrieval, using MYC and phospho-AKT antibodies at dilutions of 1:300 and 1:70 respectively. The array was stained for TP53 by Johns Hopkins Clinical Pathology following a Ventana standard protocol. The TMA was scored by intensity (scale of 0 to 2) and percentage stained; an H-score was calculated by multiplying intensity by percentage of cells positive.

Gene expression analysis

RNA was extracted from cells and xenograft tumors using TRIZOL according to manufacturer's directions. RNA was assessed for quality and integrity using a Bioanalyzer (Agilent Technologies) and samples had a RNA Integrity Number score of higher than 8.2 (25). Gene expression data was generated using Affymetrix High Throughput (HT) U1332+ Chip (Santa Clara, CA) according to manufacturer's guidelines. Raw data was processed and analyzed using GenePattern as previously described (12, 26). The dataset will be made available as dataset GSE77475 at GEO (Gene Expression Omnibus).

In vitro Drug Treatments

Palbociclib was purchased from Sellekchem and diluted in water according to manufacturer's instructions.

DiSCoVER Analysis Method

The main analysis components of DiSCoVER are shown in Supplementary Figure 2. The murine xerographs of transformed hNSC G3 samples and controls were profiled using Affymetrix arrays (see Gene expression analysis above). The gene probe identifiers were mapped into gene symbols using the *Collapse Dataset* tool ("max probe") of the GSEA software (27). The top 150 up-regulated genes between the murine xenographs of transformed hNSC G3 samples and controls were used to create an hNSC G3 oncogenic transcriptional signature (Supplementary Table 1). We used this gene set to project two large mRNA expression datasets, The Cancer Cell Line Encyclopedia (CCLE) (28) and the Sanger Dataset (29). This projection is made using single-sample GSEA (30) to produce enrichment profiles of the hNSC G3 signature in each sample of those datasets. Once this projection is completed we match the signature profile vs. drug sensitive profiles corresponding to drug sensitivity datasets: The Cancer Therapeutics Response Portal (CTRP v2) (31), the CCLE Pharmacological Profiling Drug Data (28); and The Genomics of Drug Sensitivity in Cancer (29). Therefore there are three comparisons we performed between the transcriptional profile of the hNSC G3 signature and the drug sensitivity profiles (see Supplementary Figure 1 Comparison I, II and III). There are only two mRNA datasets because the CCLE and CTRP v2 sensitivity datasets share the same mRNA samples. The matching scores between the signature, and each drug sensitivity profile, were computed using the Information Coefficient (IC), an information theoretic-measure of association, similar to the measure of association we used in Abazeed *et al.* 2013 (32) to compare radiation sensitivity vs. pathway expression. Once we obtained the matching scores of each drug against the hNSC G3 signature, we performed a permutation test on the signature profile with 10,000 permutations. These values are used to create an empirical null distribution from which nominal p-values and False Discovery Rates (FDR) (33) are computed. We focus in the top scoring compounds with FDR below 0.33 in the three comparisons and look for overlaps in compounds or compound classes (Supplementary Table 2). This is the way we noticed the appearance of CDK inhibitors for each dataset (Figure 4B and Supplementary Figure 2). In Supplementary Figure 2 we show that CDK inhibitors are top hits in the 3 drug sensitivity datasets by plotting the Information score (IC) in the y-axis and the correlation coefficient (between signature and drugs) in the x-axis. This comparison of correlation vs. information

coefficients provides supplementary information about how linear or non-linear is the relationship between the signature and a given drug. The DiSCoVER method will be made publicly available as an analysis module in GenePattern.

Immunofluorescence

BrdU incorporation and cleaved caspase-3 assays were performed as described (34).

Western Blot

Protein was extracted by lysing cell pellets with RIPA buffer and quantified using a Bradford Assay. Antibodies against GAPDH (6C5: sc-32233) and Actin (C4: sc-47778) are from Santa Cruz Biotechnology®. Antibodies for total Rb (#9309), Phospho-Rb Ser780 (#8180), Phospho-Rb Ser807/811 (#8516), and cleaved-PARP (#5625) are from Cell Signaling Technology. The Nestin (10C2, MAB5326) and SOX2 antibodies are from Millipore. The following antibody dilutions were used: GAPDH (1:1000), Actin (1:1000), GFAP (1:2000), Sox2 (1:200), Nestin (1:1000), total Rb (1:1000), phospho-Rb Ser780 (1:1000), phospho-Rb Ser807/811 (1:1000), and cleaved-PARP (1:800). Peroxidase labeled secondary antibodies were diluted 1:5000 and are from KPL or Cell Signaling Technologies. Quantification was performed using ImageJ.

Animal Studies

“Principles of laboratory animal care” (NIH publication No. 8623, revised 1985) was followed, using a protocol approved by the Johns Hopkins Animal Care and Use Committee, in compliance with the United States Animal Welfare Act regulations and Public Health Service Policy. Orthotopic brain xenografting was performed as described (23). Palbociclib was prepared in a pH 4.0 50mM sodium lactate solution and administered by oral gavage in a 100uL bolus. Animals received a 150mg/kg dose 5x a week, which is a widely used dosing schedule in pre-clinical murine xenograft models (35–38). All animals were monitored daily. Symptomatic animals were euthanized and their brains removed and fixed in formalin.

Results

Group 3 primary medulloblastoma tumors express MYC, phospho-AKT, and TP53

To generate a genetically defined model of aggressive medulloblastoma, we began with human neural stem and progenitor cells obtained as described in (22) (Figure 1A, B). These cells express the stem cell marker CD133 and the neural stem cell markers NESTIN, SOX2, and GFAP (Figure 1C).

We used a tissue microarray (TMA) containing 65 primary human medulloblastoma samples that was previously characterized with respect to subgroup (9) to interrogate the expression of oncogenic elements associated with Group 3/C1 medulloblastoma. Group 3 tumors are known to overexpress *MYC* at the mRNA level (8), but MYC protein expression has not been extensively investigated in primary tumors. Immunohistochemical analysis of MYC on our TMA showed that expression was highest in Group 3 tumors (Figure 1D), with 50% expressing MYC, while only 27% of SHH tumors and 6% of Group 4 tumors had detectable MYC protein levels.

In addition to MYC, Group 3 samples had significantly higher expression of TP53 (Figure 1E), indicating dysfunction of the p53 pathway. Among Group 3 tumors, 56% were positive for increased TP53 expression, while only 25% of SHH tumors and 23% of Group 4 tumors were positive for TP53. Our group has demonstrated that anaplastic medulloblastoma tumors have elevated TP53 expression (39, 40), suggesting inactivation of the p53 pathway. We and others have shown that increased TP53 protein levels or p53 mutations are associated with worse clinical outcomes in a subgroup-dependent fashion (41).

We next investigated the expression of phospho-AKT as an indicator of mTOR status. The mTOR pathway is active in multiple medulloblastoma subgroups, including Group 3 and is associated with increased metastasis (42). We identified increased phospho-AKT staining in all subgroups represented in our TMA. Although there was a trend for increased AKT signaling in Group 3, it did not reach statistical significance (Figure 1F). In addition to MYC, TP53 and phospho-AKT, human telomerase (hTERT) has been identified as being highly expressed in embryonal tumors, and was included as a transforming element (43, 44).

Neural stem cells transduced with MYC, dominant-negative TP53, hTERT, and AKT form aggressive tumors that phenocopy Group 3 medulloblastoma

The addition of MYC alone or with constitutively active (myristolated) AKT, dominant-negative TP53 (DNp53) and human telomerase (hTERT) increases proliferation compared to normal neural stem cells and to cells immortalized with SV40 (Figure 2A). The human MYC transformed cells were *ATOH* negative (data not shown), consistent with prior murine models of MYC-driven medulloblastoma (14). Cerebellar derived neural stem and progenitor cells transduced with DNp53, MYC, AKT, and hTERT formed aggressive tumors when injected into the brains of nude mice (Figure 2B). Cerebellar stem cells immortalized with SV40 did not form tumors (Figure 1B).

The tumors expressed TP53, MYC, and phospho-AKT, indicating that these oncogenic elements used to drive transformation were maintained (Figure 2C). Tumors formed by cells transduced with all four oncogenic elements also had anaplastic features (Figure 2D i) and could spread to the leptomeningeal space (Figure 2D ii). Approximately 20% of mice had spinal metastases (Figure 2D iii). Metastasis is associated with Groups 3 and 4, the most aggressive subgroups of medulloblastoma (45). The DNTP53 hTERT AKT MYC orthotopic xenografts expressed NESTIN and MAP2 and were negative for GFAP (Figure 2E), indicating a primarily progenitor and neuronal phenotype consistent with medulloblastoma. Because no effective antibody exists for hTERT immunohistochemistry, we verified high-level expression of this hallmark in our 4-gene transduced cells by qPCR (data not shown).

Human neural stem cell models of Group 3 medulloblastoma share mRNA expression profile with human primary tumors

To further confirm that our model replicates Group 3 medulloblastoma, we performed Affymetrix mRNA expression profiling on our human cerebellar neural stem and progenitor cell models and two of our DNTP53 hT AKT MYC tumor orthotopic xenografts. Specifically, we examined the expression of 32 pathways that have been previously associated with each of the six Cho subgroups (13). High expression of a specific subset of

each of these 32 pathways is characteristic of each subgroup. We performed single-sample gene-set enrichment analysis (ssGSEA) on our model in culture and as xenografts to obtain an enrichment score for each of the medulloblastoma associated pathways. This analysis was also performed for the primary medulloblastoma tumor dataset of Tamayo *et al.* 2011 (13), allowing us to compare the profiles of our xenografts and cultured cells against human medulloblastoma tumors. The pathway enrichment profile of our cells and xenografts closely matches the profile of C1 primary tumors, the most aggressive subclass of patients within MYC-driven Group 3 (12) (Figure 3A). Samples from cells transduced with only MYC expressed the Group 3 associated mRNAs and corresponding pathway enrichment (Figure 3B). The addition of DNp53, hT and AKT to MYC increased the expression of these Group 3 associated pathways (Figure 3B). The orthotopic xenografts of cells transduced with MYC, DNp53, hT and AKT most highly express the Group 3 associated mRNAs (Figure 3B).

We also generated an association matrix that compares the pathway enrichment scores of xenografts and cell models against each tumor subtype (Figure 3C). The association is estimated using the Information Coefficient, an information-theoretical counterpart to the correlation coefficient (see methods). Primary cultures of untransduced cerebellar neural stem and progenitor cells associate most closely with the C6/WNT subgroup. The sequential addition of MYC, TP53, hTERT and AKT increases the association with the C1 subtype. Growth of these cells as orthotopic xenograft tumors further increases the association with the subtype C1 (Fig 3C).

Analysis of drug sensitivity databases with a profile created by analyzing the human neural stem cell model of Group 3 medulloblastoma reveals CDK inhibitors as a potential therapeutic target

The human neural stem cell model of medulloblastoma was used as a test subject for a novel computational analysis technique, DiSCoVER (Disease-model Signature vs. Compound-Variety Enriched Response), that we briefly describe here (additional details in methods). We created a gene set called the “hNSC G3 signature” of the 150 most up-regulated genes in the murine xerographs of human neural stem cell line transformed with DN- p53, hTERT, constitutively active AKT and MYC (Supplementary Table 1). We then analyzed the gene expression datasets of two mRNA datasets (see methods) using single-sample gene set enrichment analysis (ssGSEA). This analysis allowed us to obtain a hNSC G3 signature enrichment score for each sample in the two mRNA datasets. We then matched the signature enrichment scores against drug sensitivity profiles that have been generated for the same samples. In this way, we identified compounds that killed cells sharing a high hNSC G3 enrichment score. We performed this comparison against three different drug sensitivity datasets and looked for overlaps in the top scoring compounds or their compound varieties. A summary of the procedure is shown in Figure 4A and the full workflow can be seen found in Supplementary Figure 1.

In this analysis we focused on the top scoring compounds with False Discovery Rates (FDR) below 0.33 (see Supplementary Table 2 and Supplementary Figure 2). The overlap analysis across datasets revealed that cancer cell lines that highly express the hNSC G3 signature are

sensitive to the cyclin-dependent kinase inhibitors (Figure 4B and Supplementary Fig S2). These inhibitors include the pan-CDK inhibitor Flavopiridol/Alvocidib (PubChem CID: 5287969) (46), CDK 1/2/5/7 inhibitor CGP-60474 that was developed as a PKC inhibitor (PubChem ID: 644215) (47), CDK4 inhibitor CGP-082996 (PubChem CID: 24825971), and the CDK4/6 inhibitor PD-0332991/Palbociclib (PubChem ID: 5330286) (35). MYC expression is known to increase the expression of cyclin-dependent kinases, so CDK inhibition is biologically congruent with the *in silico* screen (48).

The CDK4/6 inhibitor palbociclib decreases proliferation in the human neural stem cell model of medulloblastoma and patient-derived medulloblastoma cell lines

Of the CDK inhibitors identified by the DiSCoVER analysis, we decided to test palbociclib (PD-0223991) because of its clinical relevance. In addition to cerebellar neural stem cells transformed with MYC, DNp53, AKT and hT, we used cerebellar neural stem cells transformed with MYC alone and two patient-derived medulloblastoma lines (D425Med and D283Med) to test the effects of palbociclib on medulloblastoma. Inhibition of CDK4/6 activity prevents the phosphorylation of the retinoblastoma protein (Rb) (35). Western blotting showed that 5uM palbociclib treatment led to a decrease in phosphorylation of Rb at two different phosphorylation sites (Ser780, and Ser807/811). Phosphorylation at S780 decreased by 96% in cells transformed with MYC alone, by 62% in cells transformed with all four oncogenes, by 24% in D425Med cells, and by 33% in D4283Med cells. The phosphorylation at S807/811 decreased by 99% in MYC alone cells, 55% in cells transformed with all four oncogenes, by 33% in D425Med cells and by 43% in D283Med cells. (Figure 5A).

Palbociclib treatment caused a significant decrease in proliferation in all four medulloblastoma models, as determined by BrdU incorporation (Figure 5B). Palbociclib treatment for 72h caused the percentage of BrdU positive cells to drop from 32% to 12% in D425Med ($p=0.000004$ by Student's t-test), from 40% to 21% in D283Med ($p=0.004$ by Student' t-test), from 41% to 3% in cells transformed with MYC alone ($p=0.00000009$ by Student's t-test), and from 30% to 13% in cells transformed with all four oncogenic elements ($p=0.02$ by Student's t-test). In cells immortalized with SV40, palbociclib caused a non-significant decrease in BrdU incorporation—34% 24% ($p=0.06$ by Student's t-test) (Figure 5B). The pan-CDK inhibitor flavopiridol, which was also identified by DiSCoVER, also decreased proliferation in MYC-driven cell lines and MYC-transduced neural stem cells (Supplementary Figure 3A).

Palbociclib induces apoptosis in human MYC-driven medulloblastoma

Treatment of our MYC-driven human models of medulloblastoma with 5uM of palbociclib for 72h caused the percentage of cleaved caspase-3 positive cells in to increase from 6% to 21% in D425Med ($p=0.0005$ Student's t-test), from 3% to 9% in D283Med ($p=0.001$ Student's t-test), from 20% to 70% in cells immortalized with MYC alone ($p=0.0000004$ Student's t-test) and from 21% to 45% in cells transformed with all four oncogenic elements ($p=0.000002$ by Student's t-test) (Figure 5B). In SV40 immortalized cells, palbociclib caused a non-significant increase in the percentage of cleaved-caspase 3 positive cells—10% to 15% ($p=0.14$ by Student's t-test) (Figure 5C). Treatment with 1 or 5uM of palbociclib for

24h caused an increase in the expression of cleaved-PARP (as measured by Western blotting), indicating increased levels of apoptosis (Figure 5D). Similar to palbociclib, flavopiridol also caused an increase in apoptosis (Supplementary Figure 3B).

Palbociclib significantly improves survival of mice with medulloblastoma orthotopic xenografts

We next tested the efficacy of palbociclib as a monotherapy *in vivo*. Palbociclib treatment has been shown to increase survival in a mouse models of brainstem glioma and GBM (36, 37). Palbociclib treatment significantly extended survival of mice with D425Med intracranial xenografts by 48%--from 25 to 37 days (p=0.003 by Log-rank test) (Figure 6A). To verify that palbociclib was causing this effect by inhibiting CDK function, we performed IHC for phospho-Rb on tumors from animals that were given a single dose of vehicle or palbociclib four hours prior to euthanasia. Tumors from mice given palbociclib had a significantly lower percentage of phospho-Rb positive cells compared to mice given the vehicle control (38% vs 54%, p=0.00025 by Student's t-test), indicating that the drug cross the blood brain barrier and penetrates the tumor (Figure 6B). Images of two tumors from mice given vehicle are in Figure 6C, left. Images of two tumors from mice given palbociclib are in Figure 6C, right.

Discussion

Group 3 medulloblastoma is a highly lethal disease. Our human neural stem and progenitor cell model phenotypically, histologically and genetically mimics the C1 component of Group 3, the most lethal sub-group of medulloblastoma (13). Although our model shares MYC activation and p53 pathway inhibition with murine neural stem cell systems created by Pei *et al.* and Kawauchi *et al.*, the addition of activated *AKT*, which is a known driver of medulloblastoma metastasis and resistance to therapy as well as *hTERT*, which reflects the high frequency of *TERT* promoter mutations in medulloblastoma, adds a richness to our model (43, 49). The increasing fidelity of our human neural stem cells to Group 3 with the sequential addition of oncogenic elements as demonstrated in Figure 3 highlights this point. Alterations in MYC and TP53 occur together in relapsed medulloblastoma of all subtypes (17), so our cells can also serve as a model of relapsed disease.

We here present a novel method for *in silico* prediction of drug sensitivity, which we believe may significantly accelerate the identification of novel therapeutics for rare cancer types. Our DiSCoVER approach differs from existing *in silico* methods such as Connectivity MAP (C-MAP) in that DiSCoVER uses the actual drug response cell viability profiles (e.g. IC50 or AUC) of multiple drug screening datasets involving hundreds of cell lines treated with each drug, rather than the transcriptional changes, e.g. as detected by 1,000 "landmark" genes induced by drug perturbations in a few selected cell lines as it is done in CMAP. The drug screening responses are more accurate at representing the effect of a drug in terms of affecting cell viability and not only transcriptional changes that may, or may not, impinge on cell viability.

CMAP matches the gene set representing the disease signature against transcriptional profiles of drug perturbations in a few cell lines using the Kolmogorov-Smirnov enrichment

statistic. This is a useful approach in general but sometimes it does not easily allow the detection of more subtle disease vs. drug associations in a broader context involving a large number and diversity of cellular states. In DiSCoVER we first produced an enrichment score for the disease signature in each cell line (using single-sample GSEA); and then we match the pattern of these scores across hundreds of cell lines, against the drug sensitivity profiles for the same cell lines, using an information-theoretic metric of association. This approach provides a high degree of sensitivity and specificity in finding drug responses that match the disease signature, even when the relationship, i) is restricted to a few cell lines representing a relevant but narrowly represented biological state, ii) when this relationship is not strictly linear or, iii) when it is very weak. DiSCoVER also repeats the analysis in multiple external datasets and then compares the results across them, e.g. considering drug classes, and not only individual instances as occurs in CMAP.

One identified therapeutic target in our *in silico* pre-clinical drug screen was cyclin-dependent kinases. MYC plays a significant role in regulating the cell cycle through variety of mechanisms (50). Cyclin-dependent kinases, cyclins and E2F transcription factors are all directly regulated by MYC (50). MYC-driven murine lymphoma and hepatoblastoma are sensitive to CDK1/2 inhibition, further highlighting CDKs as a potential Achilles' heel in MYC-driven malignancies (51, 52). Other groups have demonstrated the use of CDK inhibitors in treating brain tumors (36, 37). Faria *et al* showed the efficacy of an investigational CDK1/5/GSK3b inhibitor, alsterpaullone, in MYC-driven medulloblastoma cell lines, though much of the tumor suppressing effect was demonstrated to be mediated through mTOR inhibition (53). Palbociclib is a CDK4/6 inhibitor approved for treatment of advanced estrogen-receptor positive breast cancers (54). Palbociclib decreased the growth of high-serum medulloblastoma cell lines *in vitro* (55). We chose an *in vivo* dose of palbociclib consistent with that given in other pre-clinical models (35–38). A phase I clinical trial of palbociclib in pediatric brain tumor patients is currently ongoing (NCT02255461), and the maximum tolerated dose has yet to be reported.

Methotrexate and cytarabine were among other top hits revealed by the DiSCoVER analysis (Supplementary Table 2). These drugs are currently in use in medulloblastoma treatment and are structurally similar to pemetrexed and gemcitabine, which were recently identified as being active in medulloblastoma xenografts (56). The identification of biologically plausible targets and compounds that are being explored by other scientists validates our *in silico* strategy of using the hNSC G3 signature to probe available datasets of drug sensitivity data.

Identification of increased apoptosis downstream of palbociclib in our cell lines and neural stem cell models differs from the standard response to CDK inhibitors, which are largely viewed as cytostatic agents in other cancer types (38, 57–60). However, in combination with cytarabine, dexamethasone, and bortezomib, palbociclib enhances cytotoxicity (38, 59, 60). In our model, palbociclib induces apoptosis as a monotherapy, so is possible that we will see synergy and enhanced cell killing when it is used in combination with other cytotoxic agents commonly used to treat in MYC-driven medulloblastoma.

In conclusion, we present a novel strategy for creating new models of tumors and for pre-clinical screening of drug targets. We created a human neural stem cell model of Group 3

medulloblastoma and used this model to screen drug sensitivity databases and validate an identified target. Palbociclib may be an effective treatment for poor-prognosis medulloblastoma in carefully selected patients. Our overall strategy of using tissue-specific human stem and progenitor cells may be useful for developing models of other tumor types.

Supplementary Material

Refer to Web version on PubMed Central for supplementary material.

Acknowledgments

Financial Support:

St. Baldrick's Foundation, Hyundai Hope on Wheels, and Giant Food Pediatric Cancer Research Fund, The Spencer Grace Foundation**,** The Deming Family, and The Children's Brain Tumor Foundation (E.H.R); NCI Core Grant to the Johns Hopkins SKCCC P30 CA006973, and R01NS055089 (to CGE), NIH R01 CA154480 (to JPM and PT), NIH R01 109467 (to JPM and SLP), NIH R01GM074024 (to JPM and PT). Comprehensive Cancer Center Freiburg (UK, JM, GN). NCI's Cancer Target Discovery and Development (CTD^2) Network U01CA176152 (S.L.S.).

References

1. Silva PB, Rodini CO, Kaid C, Nakahata AM, Pereira MC, Matushita H, et al. Establishment of a novel human medulloblastoma cell line characterized by highly aggressive stem-like cells. Cytotechnology. 2015; Epub ahead of print. doi: 10.1007/s10616-015-9914-5
2. Hughes P, Marshall D, Reid Y, Parkes H, Gelber C. The costs of using unauthenticated, over-passaged cell lines: how much more data do we need? Biotechniques. 2007; 43:575, 7–8, 81–2. passim. [PubMed: 18072586]
3. Zhao X, Liu Z, Yu L, Zhang Y, Baxter P, Voicu H, et al. Global gene expression profiling confirms the molecular fidelity of primary tumor-based orthotopic xenograft mouse models of medulloblastoma. Neuro Oncol. 2012; 14:574–83. [PubMed: 22459127]
4. Hamad NM, Elconin JH, Karnoub AE, Bai W, Rich JN, Abraham RT, et al. Distinct requirements for Ras oncogenesis in human versus mouse cells. Genes Dev. 2002; 16:2045–57. [PubMed: 12183360]
5. Northcott PA, Korshunov A, Pfister SM, Taylor MD. The clinical implications of medulloblastoma subgroups. Nat Rev Neurol. 2012; 8:340–51. [PubMed: 22565209]
6. Stearns D, Chaudhry A, Abel TW, Burger PC, Dang CV, Eberhart CG. c-myc overexpression causes anaplasia in medulloblastoma. Cancer Res. 2006; 66:673–81. [PubMed: 16423996]
7. Pfister S, Remke M, Benner A, Mendrzyk F, Toedt G, Felsberg J, et al. Outcome prediction in pediatric medulloblastoma based on DNA copy-number aberrations of chromosomes 6q and 17q and the MYC and MYCN loci. J Clin Oncol. 2009; 27:1627–36. [PubMed: 19255330]
8. Eberhart CG, Kratz J, Wang Y, Summers K, Stearns D, Cohen K, et al. Histopathological and molecular prognostic markers in medulloblastoma: c-myc, N-myc, TrkC, and anaplasia. J Neuropathol Exp Neurol. 2004; 63:441–9. [PubMed: 15198123]
9. Northcott PA, Korshunov A, Witt H, Hielscher T, Eberhart CG, Mack S, et al. Medulloblastoma comprises four distinct molecular variants. J Clin Oncol. 2011; 29:1408–14. [PubMed: 20823417]
10. Kool M, Korshunov A, Remke M, Jones DT, Schlanstein M, Northcott PA, et al. Molecular subgroups of medulloblastoma: an international meta-analysis of transcriptome, genetic aberrations, and clinical data of WNT, SHH, Group 3, and Group 4 medulloblastomas. Acta Neuropathol. 2012; 123:473–84. [PubMed: 22358457]
11. Taylor MD, Northcott PA, Korshunov A, Remke M, Cho YJ, Clifford SC, et al. Molecular subgroups of medulloblastoma: the current consensus. Acta Neuropathol. 2012; 123:465–72. [PubMed: 22134537]

12. Cho YJ, Tsherniak A, Tamayo P, Santagata S, Ligon A, Greulich H, et al. Integrative genomic analysis of medulloblastoma identifies a molecular subgroup that drives poor clinical outcome. J Clin Oncol. 2011; 29:1424–30. [PubMed: 21098324]
13. Tamayo P, Cho YJ, Tsherniak A, Greulich H, Ambrogio L, Schouten-van Meeteren N, et al. Predicting relapse in patients with medulloblastoma by integrating evidence from clinical and genomic features. J Clin Oncol. 2011; 29:1415–23. [PubMed: 21357789]
14. Pei Y, Moore CE, Wang J, Tewari AK, Eroshkin A, Cho YJ, et al. An animal model of MYC-driven medulloblastoma. Cancer Cell. 2012; 21:155–67. [PubMed: 22340590]
15. Kawauchi D, Robinson G, Uziel T, Gibson P, Rehg J, Gao C, et al. A mouse model of the most aggressive subgroup of human medulloblastoma. Cancer Cell. 2012; 21:168–80. [PubMed: 22340591]
16. Bandopadhayay P, Bergthold G, Nguyen B, Schubert S, Gholamin S, Tang Y, et al. BET bromodomain inhibition of MYC-amplified medulloblastoma. Clin Cancer Res. 2014; 20:912–25. [PubMed: 24297863]
17. Hill RM, Kuijper S, Lindsey JC, Petrie K, Schwalbe EC, Barker K, et al. Combined MYC and P53 defects emerge at medulloblastoma relapse and define rapidly progressive, therapeutically targetable disease. Cancer Cell. 2015; 27:72–84. [PubMed: 25533335]
18. Bigner SH, Friedman HS, Vogelstein B, Oakes WJ, Bigner DD. Amplification of the c-myc gene in human medulloblastoma cell lines and xenografts. Cancer Res. 1990; 50:2347–50. [PubMed: 2180567]
19. Swartling FJ, Grimmer MR, Hackett CS, Northcott PA, Fan QW, Goldenberg DD, et al. Pleiotropic role for MYCN in medulloblastoma. Genes Dev. 2010; 24:1059–72. [PubMed: 20478998]
20. Poschl J, Stark S, Neumann P, Grobner S, Kawauchi D, Jones DT, et al. Genomic and transcriptomic analyses match medulloblastoma mouse models to their human counterparts. Acta Neuropathol. 2014; 128:123–36. [PubMed: 24871706]
21. Parsons DW, Li M, Zhang X, Jones S, Leary RJ, Lin JC, et al. The genetic landscape of the childhood cancer medulloblastoma. Science. 2011; 331:435–9. [PubMed: 21163964]
22. Lopez WO, Nikkhah G, Kahlert UD, Maciaczyk D, Bogiel T, Moellers S, et al. Clinical neurotransplantation protocol for Huntington's and Parkinson's disease. Restor Neurol Neurosci. 2013; 31:579–95. [PubMed: 23777636]
23. Mao XG, Hutt-Cabezas M, Orr BA, Weingart M, Taylor I, Rajan AK, et al. LIN28A facilitates the transformation of human neural stem cells and promotes glioblastoma tumorigenesis through a pro-invasive genetic program. Oncotarget. 2013; 4:1050–64. [PubMed: 23846349]
24. Raabe EH, Lim KS, Kim JM, Meeker A, Mao XG, Nikkhah G, et al. BRAF activation induces transformation and then senescence in human neural stem cells: a pilocytic astrocytoma model. Clin Cancer Res. 2011; 17:3590–9. [PubMed: 21636552]
25. Schroeder A, Mueller O, Stocker S, Salowsky R, Leiber M, Gassmann M, et al. The RIN: an RNA integrity number for assigning integrity values to RNA measurements. BMC Mol Biol. 2006; 7:3. [PubMed: 16448564]
26. Subramanian A, Tamayo P, Mootha VK, Mukherjee S, Ebert BL, Gillette MA, et al. Gene set enrichment analysis: a knowledge-based approach for interpreting genome-wide expression profiles. Proc Natl Acad Sci U S A. 2005; 102:15545–50. [PubMed: 16199517]
27. Subramanian A, Kuehn H, Gould J, Tamayo P, Mesirov JP. GSEA-P: a desktop application for Gene Set Enrichment Analysis. Bioinformatics. 2007; 23:3251–3. [PubMed: 17644558]
28. Barretina J, Caponigro G, Stransky N, Venkatesan K, Margolin AA, Kim S, et al. The Cancer Cell Line Encyclopedia enables predictive modelling of anticancer drug sensitivity. Nature. 2012; 483:603–7. [PubMed: 22460905]
29. Yang W, Soares J, Greninger P, Edelman EJ, Lightfoot H, Forbes S, et al. Genomics of Drug Sensitivity in Cancer (GDSC): a resource for therapeutic biomarker discovery in cancer cells. Nucleic Acids Res. 2013; 41:D955–61. [PubMed: 23180760]
30. Barbie DA, Tamayo P, Boehm JS, Kim SY, Moody SE, Dunn IF, et al. Systematic RNA interference reveals that oncogenic KRAS-driven cancers require TBK1. Nature. 2009; 462:108–12. [PubMed: 19847166]

31. Seashore-Ludlow B, Rees MG, Cheah JH, Cokol M, Price EV, Coletti ME, et al. Harnessing Connectivity in a Large-Scale Small-Molecule Sensitivity Dataset. Cancer Discov. 2015; 5:1210–23. [PubMed: 26482930]
32. Abazeed ME, Adams DJ, Hurov KE, Tamayo P, Creighton CJ, Sonkin D, et al. Integrative radiogenomic profiling of squamous cell lung cancer. Cancer Res. 2013; 73:6289–98. [PubMed: 23980093]
33. Benjamini, YaHY. Controlling the False Discovery Rate: A Practical and Powerful Approach to Multiple Testing. Journal of the Royal Statistical Society Series B (Methodological). 1995; 57:289–300.
34. Weingart MF, Roth JJ, Hutt-Cabezas M, Busse TM, Kaur H, Price A, et al. Disrupting LIN28 in atypical teratoid rhabdoid tumors reveals the importance of the mitogen activated protein kinase pathway as a therapeutic target. Oncotarget. 2015; 6:3165–77. [PubMed: 25638158]
35. Fry DW, Harvey PJ, Keller PR, Elliott WL, Meade M, Trachet E, et al. Specific inhibition of cyclin-dependent kinase 4/6 by PD 0332991 and associated antitumor activity in human tumor xenografts. Mol Cancer Ther. 2004; 3:1427–38. [PubMed: 15542782]
36. Barton KL, Misuraca K, Cordero F, Dobrikova E, Min HD, Gromeier M, et al. PD-0332991, a CDK4/6 inhibitor, significantly prolongs survival in a genetically engineered mouse model of brainstem glioma. PLoS One. 2013; 8:e77639. [PubMed: 24098593]
37. Michaud K, Solomon DA, Oermann E, Kim JS, Zhong WZ, Prados MD, et al. Pharmacologic inhibition of cyclin-dependent kinases 4 and 6 arrests the growth of glioblastoma multiforme intracranial xenografts. Cancer Res. 2010; 70:3228–38. [PubMed: 20354191]
38. Menu E, Garcia J, Huang X, Di Liberto M, Toogood PL, Chen I, et al. A novel therapeutic combination using PD 0332991 and bortezomib: study in the 5T33MM myeloma model. Cancer Res. 2008; 68:5519–23. [PubMed: 18632601]
39. Frank AJ, Hernan R, Hollander A, Lindsey JC, Lusher ME, Fuller CE, et al. The TP53-ARF tumor suppressor pathway is frequently disrupted in large/cell anaplastic medulloblastoma. Brain Res Mol Brain Res. 2004; 121:137–40. [PubMed: 14969745]
40. Eberhart CG, Chaudhry A, Daniel RW, Khaki L, Shah KV, Gravitt PE. Increased p53 immunopositivity in anaplastic medulloblastoma and supratentorial PNET is not caused by JC virus. BMC Cancer. 2005; 5:19. [PubMed: 15717928]
41. Zhukova N, Ramaswamy V, Remke M, Pfaff E, Shih DJ, Martin DC, et al. Subgroup-specific prognostic implications of TP53 mutation in medulloblastoma. J Clin Oncol. 2013; 31:2927–35. [PubMed: 23835706]
42. Mumert M, Dubuc A, Wu X, Northcott PA, Chin SS, Pedone CA, et al. Functional genomics identifies drivers of medulloblastoma dissemination. Cancer Res. 2012; 72:4944–53. [PubMed: 22875024]
43. Fan X, Wang Y, Kratz J, Brat DJ, Robitaille Y, Moghrabi A, et al. hTERT gene amplification and increased mRNA expression in central nervous system embryonal tumors. Am J Pathol. 2003; 162:1763–9. [PubMed: 12759234]
44. Killela PJ, Reitman ZJ, Jiao Y, Bettegowda C, Agrawal N, Diaz LA Jr, et al. TERT promoter mutations occur frequently in gliomas and a subset of tumors derived from cells with low rates of self-renewal. Proc Natl Acad Sci U S A. 2013; 110:6021–6. [PubMed: 23530248]
45. Ramaswamy V, Remke M, Bouffet E, Faria CC, Perreault S, Cho YJ, et al. Recurrence patterns across medulloblastoma subgroups: an integrated clinical and molecular analysis. Lancet Oncol. 2013; 14:1200–7. [PubMed: 24140199]
46. Kaur G, Stetler-Stevenson M, Sebers S, Worland P, Sedlacek H, Myers C, et al. Growth inhibition with reversible cell cycle arrest of carcinoma cells by flavone L86-8275. J Natl Cancer Inst. 1992; 84:1736–40. [PubMed: 1279187]
47. Stanetty P, Hattinger G, Schnurch M, Mihovilovic MD. Novel and efficient access to phenylamino-pyrimidine type protein kinase C inhibitors utilizing a Negishi cross-coupling strategy. J Org Chem. 2005; 70:5215–20. [PubMed: 15960526]
48. Mateyak MK, Obaya AJ, Sedivy JM. c-Myc regulates cyclin D-Cdk4 and -Cdk6 activity but affects cell cycle progression at multiple independent points. Mol Cell Biol. 1999; 19:4672–83. [PubMed: 10373516]

49. Weeraratne SD, Amani V, Teider N, Pierre-Francois J, Winter D, Kye MJ, et al. Pleiotropic effects of miR-183~96~182 converge to regulate cell survival, proliferation and migration in medulloblastoma. Acta Neuropathol. 2012; 123:539–52. [PubMed: 22402744]
50. Bretones G, Delgado MD, Leon J. Myc and cell cycle control. Biochim Biophys Acta. 2015; 1849:506–16. [PubMed: 24704206]
51. Goga A, Yang D, Tward AD, Morgan DO, Bishop JM. Inhibition of CDK1 as a potential therapy for tumors over-expressing MYC. Nat Med. 2007; 13:820–7. [PubMed: 17589519]
52. Campaner S, Doni M, Hydbring P, Verrecchia A, Bianchi L, Sardella D, et al. Cdk2 suppresses cellular senescence induced by the c-myc oncogene. Nat Cell Biol. 2010; 12:54–9. 1–14. sup. [PubMed: 20010815]
53. Faria CC, Agnihotri S, Mack SC, Golbourn BJ, Diaz RJ, Olsen S, et al. Identification of alsterpaullone as a novel small molecule inhibitor to target group 3 medulloblastoma. Oncotarget. 2015; 6:21718–29. [PubMed: 26061748]
54. Turner NC, Ro J, Andre F, Loi S, Verma S, Iwata H, et al. Palbociclib in Hormone-Receptor-Positive Advanced Breast Cancer. N Engl J Med. 2015; 373:209–19. [PubMed: 26030518]
55. Whiteway SL, Harris PS, Venkataraman S, Alimova I, Birks DK, Donson AM, et al. Inhibition of cyclin-dependent kinase 6 suppresses cell proliferation and enhances radiation sensitivity in medulloblastoma cells. J Neurooncol. 2013; 111:113–21. [PubMed: 23138228]
56. Morfouace M, Shelat A, Jacus M, Freeman BB 3rd, Turner D, Robinson S, et al. Pemetrexed and gemcitabine as combination therapy for the treatment of Group3 medulloblastoma. Cancer Cell. 2014; 25:516–29. [PubMed: 24684846]
57. Dean JL, McClendon AK, Knudsen ES. Modification of the DNA damage response by therapeutic CDK4/6 inhibition. J Biol Chem. 2012; 287:29075–87. [PubMed: 22733811]
58. Finn RS, Dering J, Conklin D, Kalous O, Cohen DJ, Desai AJ, et al. PD 0332991, a selective cyclin D kinase 4/6 inhibitor, preferentially inhibits proliferation of luminal estrogen receptor-positive human breast cancer cell lines in vitro. Breast Cancer Res. 2009; 11:R77. [PubMed: 19874578]
59. Baughn LB, Di Liberto M, Wu K, Toogood PL, Louie T, Gottschalk R, et al. A novel orally active small molecule potently induces G1 arrest in primary myeloma cells and prevents tumor growth by specific inhibition of cyclin-dependent kinase 4/6. Cancer Res. 2006; 66:7661–7. [PubMed: 16885367]
60. Yang C, Boyson CA, Di Liberto M, Huang X, Hannah J, Dorn DC, et al. CDK4/6 Inhibitor PD 0332991 Sensitizes Acute Myeloid Leukemia to Cytarabine-Mediated Cytotoxicity. Cancer Res. 2015; 75:1838–45. [PubMed: 25744718]

Translational Relevance

Genetically accurate model systems are crucial to expanding our knowledge of rare tumor subtypes and to developing new therapeutics. The strategy we present here, based on adding key transformative oncogenic elements to stem cells from the tissue of a cancer's origin, could have great utility in many tumor types. Screening external existing drug sensitivity datasets provides a way to identify *in silico* candidate therapeutic agents that does not require the use of large-scale *in vitro* drug screens. Using human cerebellar-derived neural stem and progenitor cells, we created a genetically and phenotypically accurate model of the most aggressive subgroup of medulloblastoma. There is an urgent need to improve medulloblastoma treatment, especially for patients with high-risk disease. We have identified and validated CDK inhibition in general, and CDK 4/6 inhibition in particular, as a candidate therapy for treating patients with MYC-driven, aggressive Group 3 medulloblastoma.

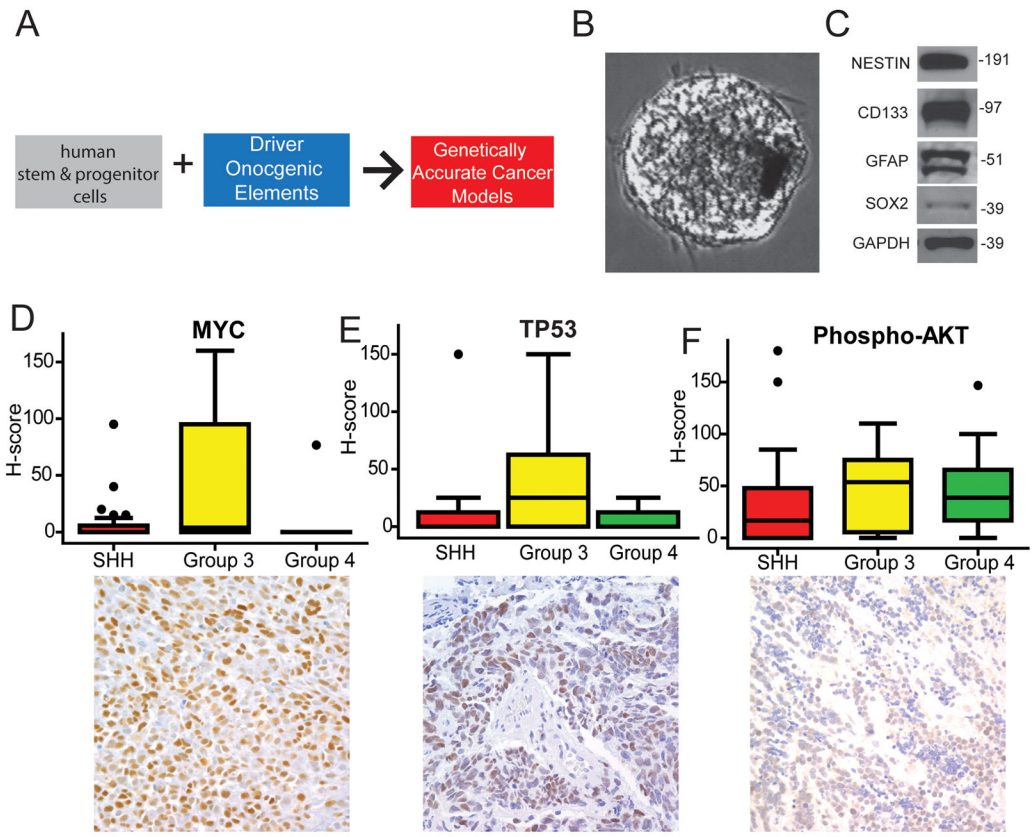

Figure 1.

A) Diagram illustrating the creation of novel cancer models using human stem cells and oncogenic elements of interest. B) Human cerebellar neurosphere. C) Western blot indicating the expression of stem cell markers in the human cerebellar neural stem and progenitor cells. D) 65-sample medulloblastoma tissue microarray (TMA) reveals that Group 3 samples have the highest MYC expression. Lower panel: an example of MYC staining in a Group 3 sample. E) Staining the TMA reveals that Group 3 samples also have the highest expression of TP53, indicating inactivation of this pathway. Lower Panel: an example of TP53 staining in a Group 3 sample. F) Phospho-AKT, which indicates activation of AKT, is expressed in all three subgroups present on the array. Lower panel: an example of Phospho-AKT staining in a Group 3 sample. Magnification of all TMA images 400x.

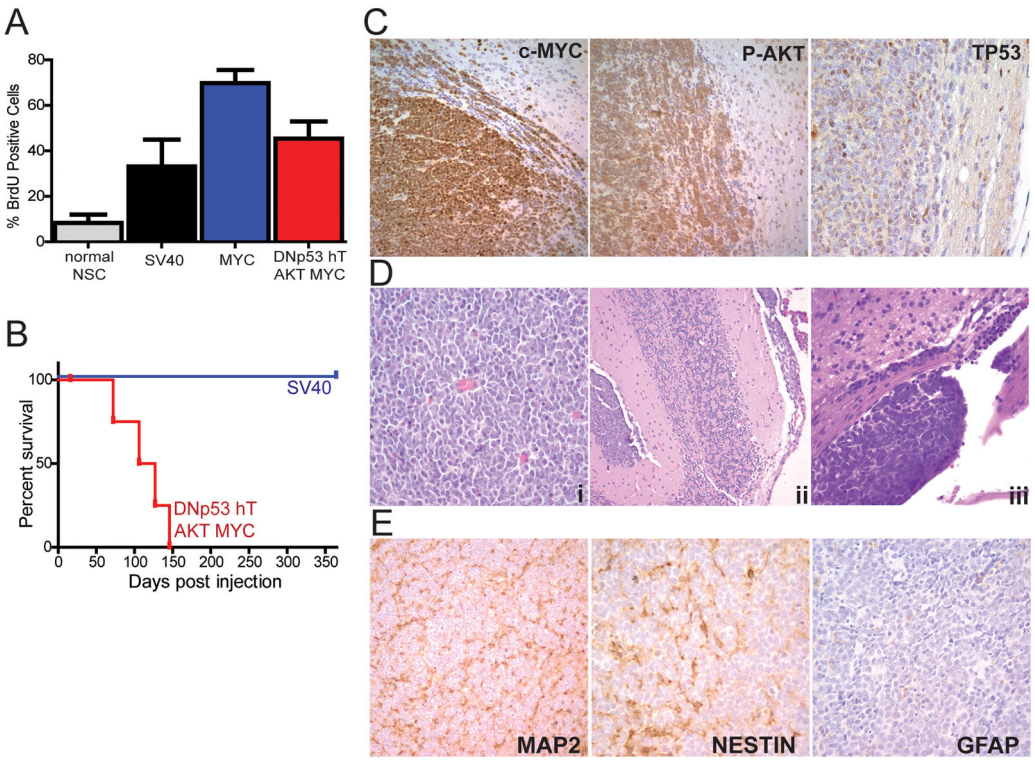

Figure 2.

A) Stem cells transduced with MYC have increased proliferation compared to untransduced neural stem cells and those immortalized with SV40. B) Cerebellar neural stem cells transduced with DN-TP53 hT AKT and MYC form tumors that kill mice in 117 days. Cells transduced with SV40 alone do not form tumors. C) These tumors express the introduced oncogenes. Images show tumor adjacent to normal brain. D) Tumors formed from cerebellar neural stem cells transduced with all four oncogenes form aggressive, anaplastic tumors (i) that spread to the leptominenges (ii) and metastasize to the spine (iii). E) The tumors are positive for MAP2 and NESTIN expression and negative for GFAP expression.

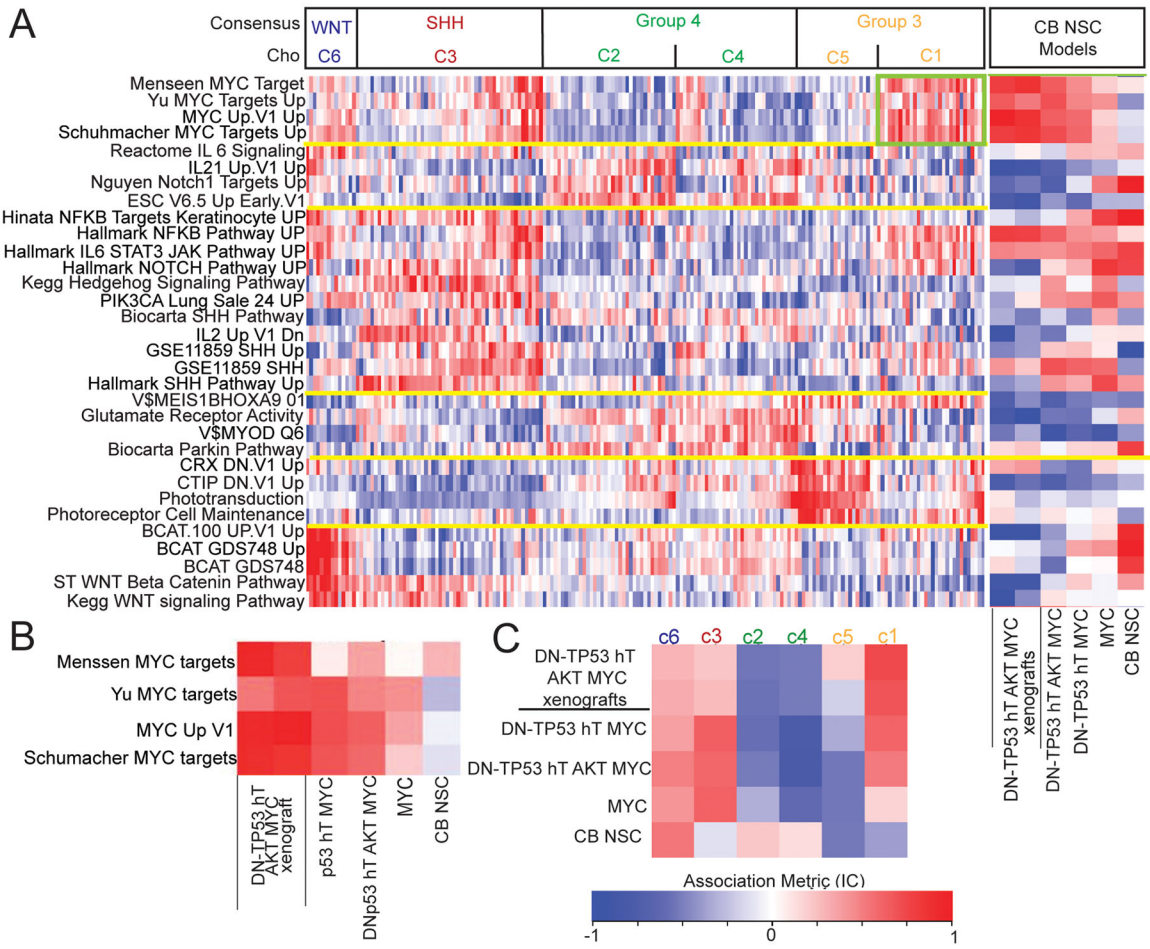

Figure 3.

Human neural stem cell models of medulloblastoma have similar expression profiles to the aggressive C1 component of Group 3. Red indicates high expression and blue indicates low expression of the pathways labeled on the left A, B. A) C1 samples have high levels of the pathways indicated by the green box. Subtype specific pathway expression profiles are separated by yellow lines. Patient expression from data from Cho *et al.*, 2011 (11). B) A close up of the human neural stem cell heat man indicates that increasing the number of oncogenes increases the expression of C1 associated pathways. The samples most highly expressing C1-associated pathways are from intracranial xenografts. C) An association metric compares the pathway enrichment subtypes (columns) to xenografts and cell models (rows). Metric is scored using Information Coefficient (IC) with red indicating higher correlation.

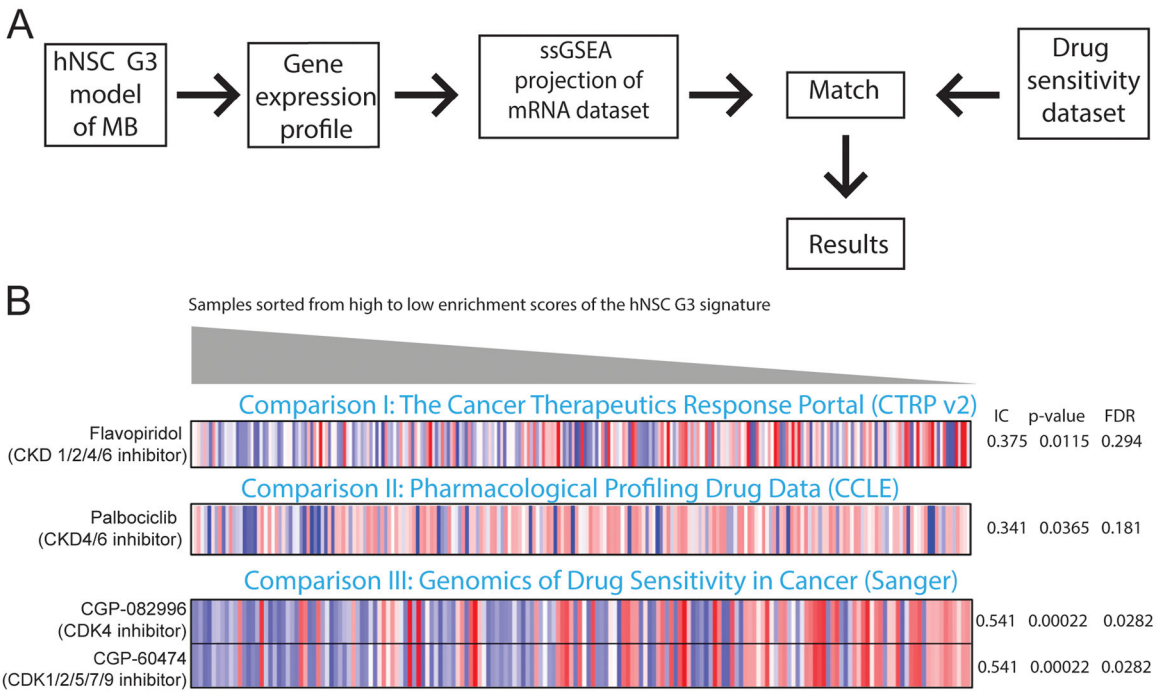

Figure 4.

A) Diagram showing a summary of the most important steps in the DiSCoVER analysis method. B) Selected cyclin-dependent kinase inhibitor results from the 3 drug sensitivity datasets. The samples are sorted from high to low enrichment scores of the hNSC G3 signature as indicated by the grey bar. The heatmaps indicate relative viability, and thus sensitivity, with blue indicating sensitivity to the indicated drug (less viable) and red indicating resistance to the indicated drug (more viable). Cells expressing a high level of the hNSC G3 signature tend to be more sensitive to these compounds. Values on the right show Information Coefficient (IC), the nominal p-value and the False Discovery Rate (FDR).

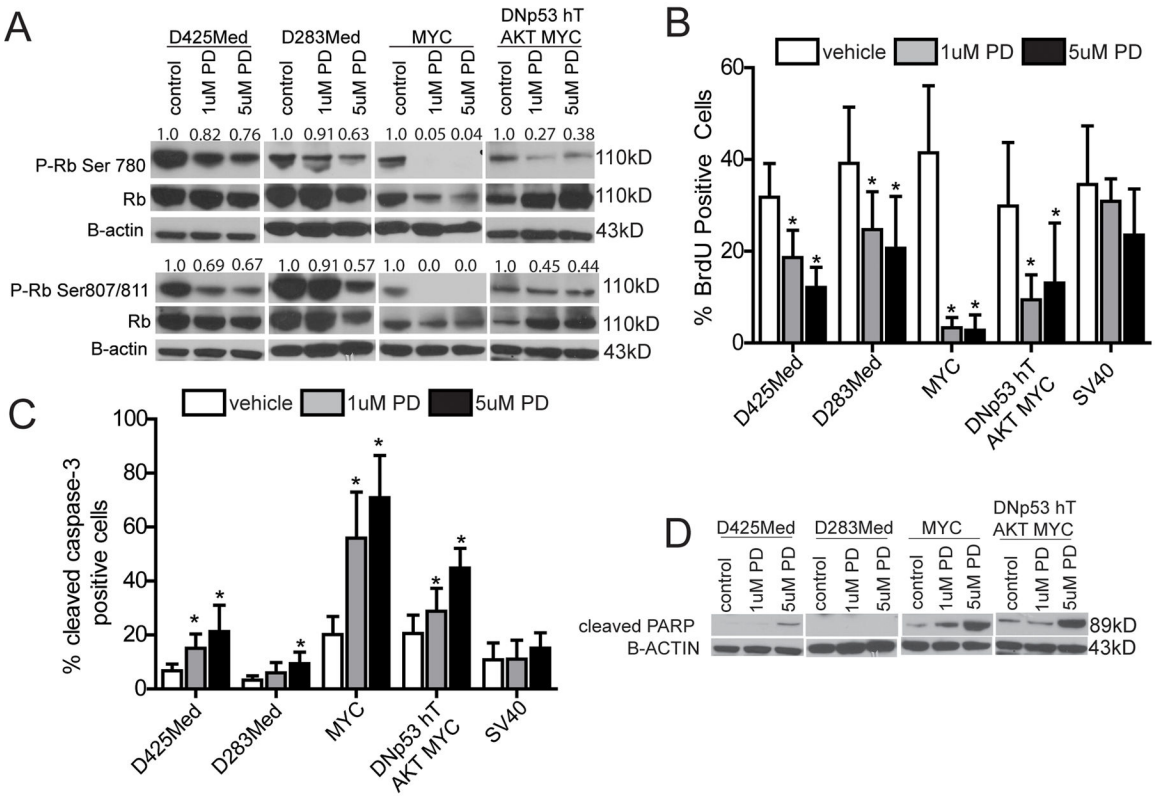

Figure 5.

A) 24h treatment with palbociclib causes decreased phosphorylation of Rb in D425Med, D283Med, cerebellar derived human neural stem cells transformed with four oncogenes and neural stem cells transformed with only MYC. SV40 immortalized cells were not included because Rb function is disabled by the large T antigen. Numbers represent the level of Rb phosphorylation as a percentage of total Rb normalized to the control. All values were also normalized to Actin. Quantification performed in ImageJ. B) 72h treatment of the CDK4/6 inhibitor palbociclib (PD) causes decreased proliferation in MYC-expressing medulloblastoma cell lines as determined by BrdU incorporation. BrdU incorporation was determined by immunofluorescence. Results are from 3 independent experiments. Bars show mean and SD. *p<0.05 by Student's t-test. C) PD treatment (72h) induces apoptosis. Apoptosis was determined by immunofluorescent staining for cleaved caspase-3. Results are from 3 independent experiments. Bars show mean and SD. *p<0.05 by Student's t-test. D) 24h PD treatment causes increased expression of cleaved-PARP, indicating cell death by apoptosis.

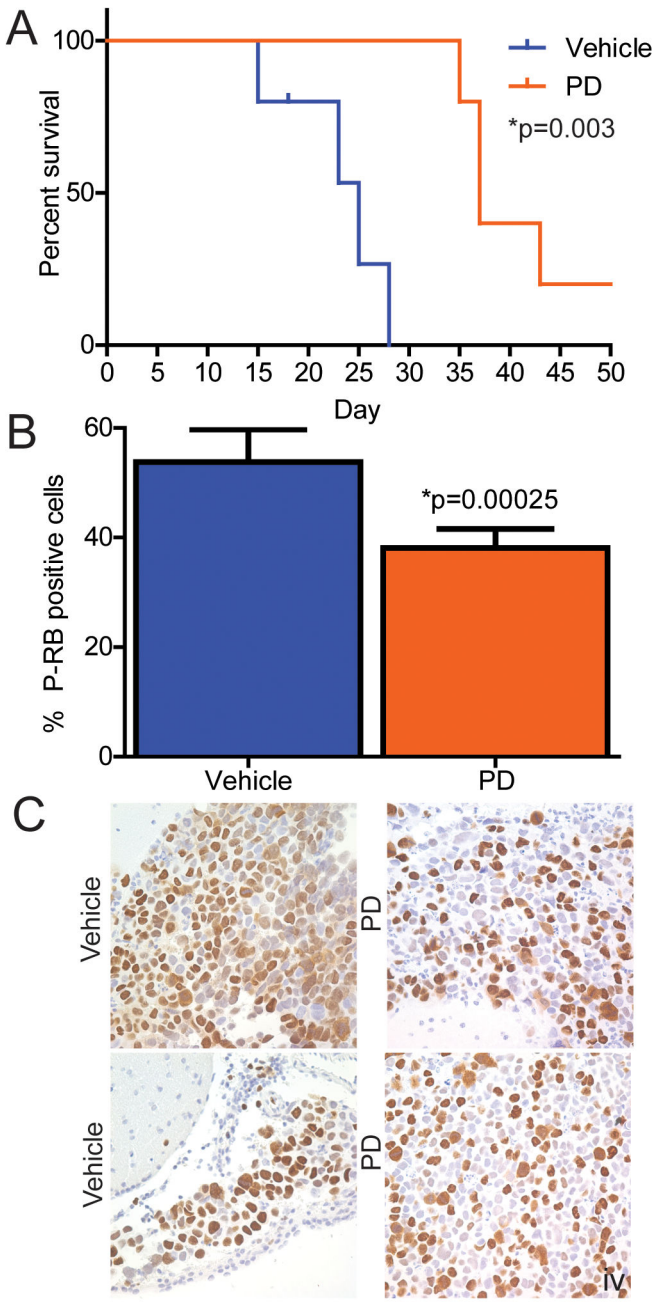

Figure 6.

A) Palbociclib treatment (150mg/kg 5x per week) significantly increases survival of mice with D425Med orthotopic xenografts. *p=0.00025 by Log-rank Test B) One 150 mg/kg dose of palbociclib deceased the percentage of phospho-Rb positive cells in D425Med xenografts from 53% to 38%. Mice were euthanized 4h post dosing. C) IHC for phospho-Rb. Left column shows tumors from two separate animals treated with vehicle. Right column shows tumors from two separate animals treated with a single dose of 150mg/kg 4h prior to euthanasia. Magnification = 400X.